Bioactive Materials 6 (2021) 2870–2880

Contents lists available at ScienceDirect

Bioactive Materials

journal homepage: www.sciencedirect.com/journal/bioactive-materials

HIF1α epigenetically repressed macrophages via CRISPR/Cas9-EZH2 system for enhanced cancer immunotherapy

Yan Dong [a,1], Siyan Zhang [b,c,d,1], Xiaotong Gao [a,1], Dandan Yin [a], Tingting Wang [c,d], Zhelong Li [b], Zhuo Wan [a], Mengying Wei [c,d], Ying Luo [e,*], Guodong Yang [c,d,**], Li Liu [a,***]

[a] Department of Hematology, Tangdu Hospital, Fourth Military Medical University, Xi'an, 710038, People's Republic of China
[b] Department of Ultrasound Diagnostics, Tangdu Hospital, Fourth Military Medical University, Xi'an, 710038, People's Republic of China
[c] State Key Laboratory of Cancer Biology, Fourth Military Medical University, Xi'an, 710032, People's Republic of China
[d] Department of Biochemistry and Molecular Biology, Fourth Military Medical University, Xi'an, 710032, People's Republic of China
[e] Department of Pathophysiology, Fourth Military Medical University, Xi'an, 710032, People's Republic of China

ARTICLE INFO

Keywords:
Cancer immunotherapy
Immune suppressive microenvironment
Macrophage
HIF1α
CRISPR/dCas9
Epigenetically reprogrammed macrophage

ABSTRACT

Immune suppressive microenvironment in tumor emerges as the main obstacle for cancer immunotherapy. In this study, we identified that HIF1*α* was activated in the tumor associated macrophages and acted as an important factor for the immune suppressive microenvironment. Epigenetically silencing of *Hif1α* via histone H3 methylation in the promoter region was achieved by CRISPR/dCas9-EZH2 system, in which histone H3 methylase EZH2 was recruited to the promoter region specifically. The *Hif1α* silenced macrophage, namely HERM (*Hif1α* Epigenetically Repressed Macrophage) manifested as inheritable tumor suppressing phenotype. In the subcutaneous B16-F10 melanoma syngeneic model, intratumoral injection of HERMs reprogrammed the immune suppressive microenvironment to the active one, reducing tumor burden and prolonging overall survival. Additionally, HERMs therapy remarkably inhibited tumor angiogenesis. Together, our study has not only identified a promising cellular and molecular target for reverting immune suppressive microenvironment, but also provided a potent strategy for reprogramming tumor microenvironment via epigenetically reprogrammed macrophages.

1. Introduction

Immunotherapy emerges as a promising strategy for cancer treatment and revolutionizes the clinical management of multiple cancers including melanoma. The main mechanism of immunotherapy is to change the tumor microenvironment so that the immune system can function to kill tumor cells [1,2]. In the tumor microenvironment, infiltrated immune cells together with stromal cells, contribute to increasing immune checkpoints, which inactivate effector T cell and have long been considered as the main obstacles for immunotherapy [3,4].

Among these immune cells, tumor associated macrophages (TAMs) represent key regulators of the complex interplay between the immune system and cancer [5]. Similar to the normal macrophages, TAMs can also be classified as two major polarized states: M1-like TAMs are activated by Th1 cytokines (such as IFNγ) and have remarkable tumoricidal effects and phagocytosis. In contrast, M2-like TAMs are activated by Th2 cytokines (including IL-4 and IL-13) and generally suppress antitumor immunity [6–8]. TAMs have great plasticity in response to variable microenvironmental stimuli. Hypoxia, a condition where the oxygen

Peer review under responsibility of KeAi Communications Co., Ltd.

* Corresponding author. Department of Pathophysiology, Fourth Military Medical University, Changlexi Road NO.169th, 710032, Xi'an, People's Republic of China.

** Corresponding author. Department of Biochemistry and Molecular Biology, Fourth Military Medical University, Changlexi Road NO.169th, 710032, Xi'an, People's Republic of China.

*** Corresponding author. Department of Hematology, Tangdu Hospital, Fourth Military Medical University, Xinsi Road NO.569th, 710032, Xi'an, People's Republic of China.

E-mail addresses: luoying@fmmu.edu.cn (Y. Luo), yanggd@fmmu.edu.cn (G. Yang), liuli1@medmail.com.cn (L. Liu).

[1] These authors contributed equally to this study.

https://doi.org/10.1016/j.bioactmat.2021.02.008
Received 10 December 2020; Received in revised form 5 February 2021; Accepted 6 February 2021

pressure is less than 5–10 mmHg, represents a hallmark feature of neoplastic growth and has profound influences on the recruitment, migration and gene expression of TAMs [9,10]. For example, hypoxic microenvironment has been found to inhibit the anti-tumoral effect of macrophage and promotes production of immunosuppressive cytokines [11].

Currently, targeted depletion of TAMs, inhibiting their recruitment and reprogramming of cell polarization are three commonly used strategies to enhance cancer immunity [8]. Compared with depletion and recruitment inhibition, TAMs reprogramming holds the capacity of providing an opportunity to revert the immune suppressive microenvironment to anti-tumoral one [12–14]. Anti-CD47 antibodies with the function of blocking the binding of CD47 to SIRPα which greatly increase phagocytosis of cancer cells, present as an efficient strategy of TAMs reprogramming [15,16]. Harnessing metabolic interventions emerges as a compensatory strategy to reprogram TAMs [17]. Additional identification of the dominant key factors determining the TAM fates is prerequisite for the reprogramming.

As to the TAM reprogramming, epigenetic engineering emerges as a promising strategy. Millions of epigenetic marks have been identified across the human genome for many human cell types and tissues [18], which become a key to discover plenty of associations at the level of gene regulation and expression, cell identity, aging and even disease, especially like cancers [19]. Additionally, epigenetic changes of cells are inheritable but also reversible [20]. In recent years, epigenome editing based on CRISPR/Cas9, an easily programmable genome editing technology, has renewed epigenetic editing, widen their therapeutic applications, and provided a safe and steady cell editing strategy [21].

In this study, we first identified that HIF1α was activated in the tumor associated macrophages and acted as an important factor for the immune suppressive microenvironment. Then, we developed a new strategy to stably silence HIF1α expression by recruiting EZH2 specifically to the promoter via CRISPR/dCas9 system. In a melanoma syngeneic models, we revealed that the engineered macrophages, namely HERMs, prevent immune evasion and enhance the anti-tumoral activities of immune system.

2. Results and discussion

2.1. TAMs are featured of Hif1α activation in advanced melanoma syngeneic model

C57BL/6 mice were inoculated with 5×10^5 B16-F10 cells and the tumor size was monitored. The tumor mass was small till 8 days, while the tumor mass was relatively large at 28 days after tumor implantation (Fig. 1A). There were abundant inflammatory cells infiltrated in the tumor of large size, compared with that in the tumor of small size (Fig. 1B). qPCR analysis revealed that reduced expression of M1 marker *Nos2* but enhanced expression of M2 marker *Mrc1* with the tumor progression, suggesting increased macrophage, mainly M2, infiltration with tumor progression (Figure S1A, B). Furthermore, qPCR analysis revealed significantly enhanced *Hif1α* expression with tumor enlarged (Figure S1C). Hypoxia represents a hallmark feature of tumor growth [22], raising the possibility that the infiltrated TAMs might be also hypoxia in large tumor mass. HIF1α expression in the $CD68^+$ TAMs was analyzed by immunofluorescence staining in tumors of different sizes. There was an increased expression of *Hif1α* in TAMs in tumors of large size (Fig. 1C and D). We detected 6 clinical melanoma samples with different tumor sizes. Consistent with the animal model, there were also elevated expression of *Hif1α* in TAMs in patients with larger tumor size (Figure S2A, B).

To further study the correlation between TAMs polarization and tumor progression, we profiled the macrophage polarization with flow cytometry. The analysis revealed that a great population of macrophages express high CD86 (M1 marker) from day 4 to day 12 after tumor implantation (Fig. 2A and Figure S1D), which reached a maximum of about

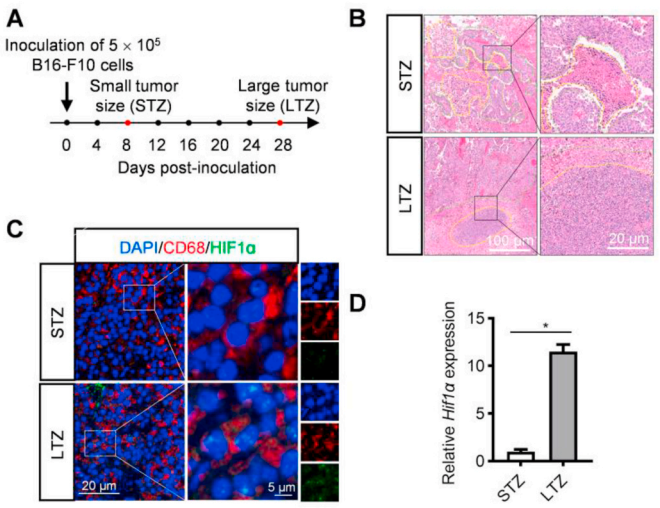

Fig. 1. Expression of HIF1α in TAMs during tumor progression in B16-F10 melanoma model. (A). Schematic of experimental design. Mice were subcutaneously injected with 5×10^5 B16-F10 cells. Tumors around 8 days post implantation were defined as small tumor size (STZ), while tumors at 28 days or later were defined as large tumor size (LTZ). (B). H&E staining of STZ and LTZ. The area circled by dotted yellow line indicates inflammatory cells and the area circled by dotted green line represent the tumor. Scale bars measure 100 μm (left) and 20 μm (right). Representative image of 4–6 mice of each group. (C). Immunofluorescence assay for co-localization of TAMs (red) and *Hif1α* (green). Nuclei were counterstained with DAPI. Scale bar, 20 μm (left) and 5 μm (right). (D). *Hif1α* mRNA expression in tumor tissues from early stage or late stage. Data are expressed as mean ± S.E.M. of three different experiments. $*p < 0.05$ by *t*-test. (For interpretation of the references to colour in this figure legend, the reader is referred to the Web version of this article.)

47% on the fourth day (Fig. 2B and Figure S1E). However, there were more macrophages with high expression of CD206 from day 12 after tumor implantation (Fig. 2A and Figure S1D), reaching a maximum of about 70% (Fig. 2C and Figure S1F). In agreement, the mRNA expression of M1 markers *Tnfα*, *Il-1β*, *Nos2* were significantly higher in tumor with small size (day 8) while M2 markers including *Arg1*, *Fizz1*, and *Mrc1* presented higher levels in the tumor with large size (day 28) (Fig. 2D, Figure S1A and Figure S1B).

Of note, the expression of *Hif1α* changed even earlier than the macrophage polarization markers (Figure S1). To explore whether *Hif1α* alters the function of macrophage under hypoxic condition, we added tumor conditioned medium to RAW264.7 cells to mirror the tumor microenvironment, followed by cobalt chloride ($CoCl_2$) treatment (Figure S3A). As expected, the protein levels of *Hif1α* was significantly elevated under hypoxic condition (Figure S3B). Moreover, hypoxia led to a slight elevated percentage of CD206 positive cells, with a maximum of about 90% (Figure S3C, E). In contrast, the percentage of CD86 positive cells was mildly downregulated under hypoxic condition (Figure S3C, D). Furthermore, the expression of *Vegfa*, *Vegfc*, growth factors related to angiogenesis and tumor progression, had a pronounced increase, while there was no significant difference of *Pdgf* expression (Figure S3F-H). Together, these data indicate that elevated expression of *Hif1α* of macrophage under hypoxic condition might contribute to tumor progression through these angiogenic factors. In other words, *Hif1α* could be a candidate to reprogram macrophage for reverse immune suppressive microenvironment.

2.2. Epigenetically silencing of HIF1α via the CRISPR/dCas9-EZH2 system

Epigenetic modification including histone methylation plays an essential role in transcription. Enhancer of zeste 2 polycomb repressive

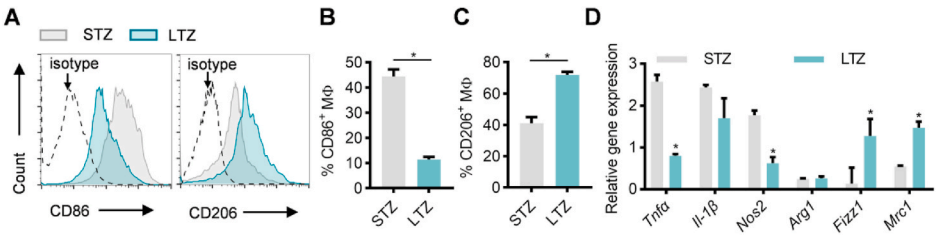

Fig. 2. Differences of TAMs in tumors with varied sizes. (A). Representative flow cytometry analysis of $CD86^+$ and $CD206^+$ macrophages in the tumor tissues of small size (STZ) and large size (LTZ). (B and C). Quantification of $CD86^+$ (B) or $CD206^+$ (C) cells (n = 5 mice/group). $^*p < 0.05$. (D). Expression levels of M1 and M2 markers in the tumor tissues of STZ and LTZ. Data are expressed as mean ± S.E.M. of three different experiments. $^*p < 0.05$ by *t*-test.

complex 2 (EZH2), a histone H3K27 methyltransferase, is the enzymatic component of the polycomb repressor complex 2 (PRC2), which controls chromatin condensation and represses gene expression [23]. Recently, structure-guided engineering of Cas9 and sgRNA based on crystallography expanded the application of CRISPR/Cas9 to activate or repress transcription [24]. We thus engineered CRISPR/Cas9, with sgRNA bearing RNA stem-loop PP7, while the interacting RNA binding protein (PCP) fused with EZH2. The resultant CRISPR/dCas9-EZH2 epigenetic editing system consisted of three components: (i) sgRNA contains two copies of PP7 stem loops embedded in the scaffold; (ii) a deactivated Cas9 surrounded by two nuclear localization signals (NLS); (iii) PCP fused with EZH2 (Fig. 3A and B and Figure S4A). The PP7 modified sgRNA scaffold can thus be recognized by PCP, which in turn recruits EZH2 to the specific DNA region targeted by the sgRNA (Fig. 3B). To test the efficiency of CRISPR/dCas9-EZH2 epigenetic editing system, macrophages were treated with dCas9-, PCP-EZH2-, and sgRNA-HIF1α-PP7-, expressing lentivirus or the controls. Western blot analysis revealed that dCas9 and PCP-EZH2 were substantially expressed in the groups infected with the corresponding lentiviruses (Fig. 3C). Meanwhile, sgRNA was extremely overexpressed after infection as expected (Figure S4C and Figure S4D). With the sgRNA targeting *Hif1α,* CRISPR-dCas9-EZH2 editing system could effectively repress *Hif1α* transcription (Fig. 3D and E). Moreover, the decrease of *Hif1α* by the CRISPR/dCas9-EZH2 targeting *Hif1α* system was stable (Figure S5). Altogether, these experiments show that the expression of *Hif1α* in macrophages could be efficiently and persistently repressed by CRISPR/dCas9-EZH2 epigenetic editing system. Hereafter, the resultant macrophages were named as HERMs (Hif1α epigenetically repressed macrophages).

2.3. Phenotype change of HERMs upon hypoxia

In view of above data, we then explored whether HERMs displayed different expression profile of the angiogenic factors. BMDMs with different lentivirus infection (Ctrl, dCas9+EZH2, dCas9+EZH2+sg-Luci, dCas9+EZH2+sg-*Hif1α*) were exposed to tumor conditioned medium and $CoCl_2$. Then, IFNγ and LPS were additionally added for M1-like polarization (Fig. 4A). Significant increase of the frequency of $CD86^+$ cells was observed in HERMs (with the lentivirus expressing dCas9, PCP-EZH2, and sg-*Hif1α*), compared with other groups (Fig. 4B and C). For M2-like polarization, IL-4 was added (Fig. 4D). Flow cytometry revealed a substantial lower of population $CD206^+$ cells *in* HERMs under hypoxic tumor microenvironment (Fig. 4E and F). Furthermore, a lower expression of growth factor *Vegfa*, *Vegfc*, and *Pdgf* were observed in HERMs compared with other groups (Fig. 4G–I). These data indicated that HERMs had significant difference with the control macrophages, and might have potent tumor-suppressive function in hypoxic tumor microenvironment.

The detection and clearance of malignant cells via macrophage phagocytosis are interfered by the tumor microenvironmental cues such as hypoxia. To explore whether the HERMs unleash the macrophage

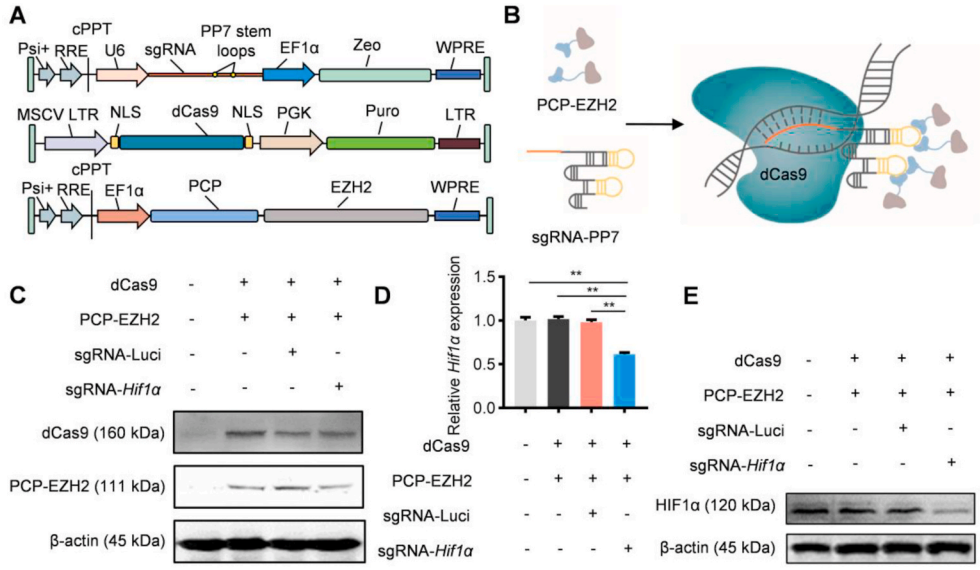

Fig. 3. Epigenetic repression of *Hif1α* via CRISPR/dCas9-EZH2 system. (A). Components of the CRISPR/dCas9-EZH2 targeting *Hif1α* system. The CRISPR/dCas9-EZH2 targeting *Hif1α* system consists of three components: (i) sgRNA with PP7 stem loops (in yellow) embedded in the scaffold (in orange) targeting *Hif1α* promoter or luciferase gene; (ii) a deactivated Cas9 (in green) surrounded by two nuclear localization signals (NLS) (in deep yellow); (iii) PP7 binding protein (in blue) combined with EZH2 (in grey). (B). Schematic illustration of the CRISPR/dCas9-EZH2 targeting Hif1α system. The sgRNA scaffold contains two copies of PP7 stem loops that protrude out of the dCas9-sgRNA complex. Dimerized PCP recognizes one PP7 stem loop which recruits four molecules of EZH2 (sgRNA + 2×PP7 + 4×PCP-EZH2). (C). Western blot analysis of dCas9 and PCP-EZH2 expression in macrophages treated as indicated. β-actin served as internal control. Images are representative of three independent experiments. (D). Expression of *Hif1α* mRNA in the bone marrow-derived macrophages (BMDMs) treated as indicated. Data are expressed as mean ± S.E.M. of three different experiments. $^{**}p < 0.01$ by one-way ANOVA. (E). Western blot analysis of HIF1α expression in BMDMs treated as indicated. Images are representative of three independent experiments. (For interpretation of the references to colour in this figure legend, the reader is referred to the Web version of this article.)

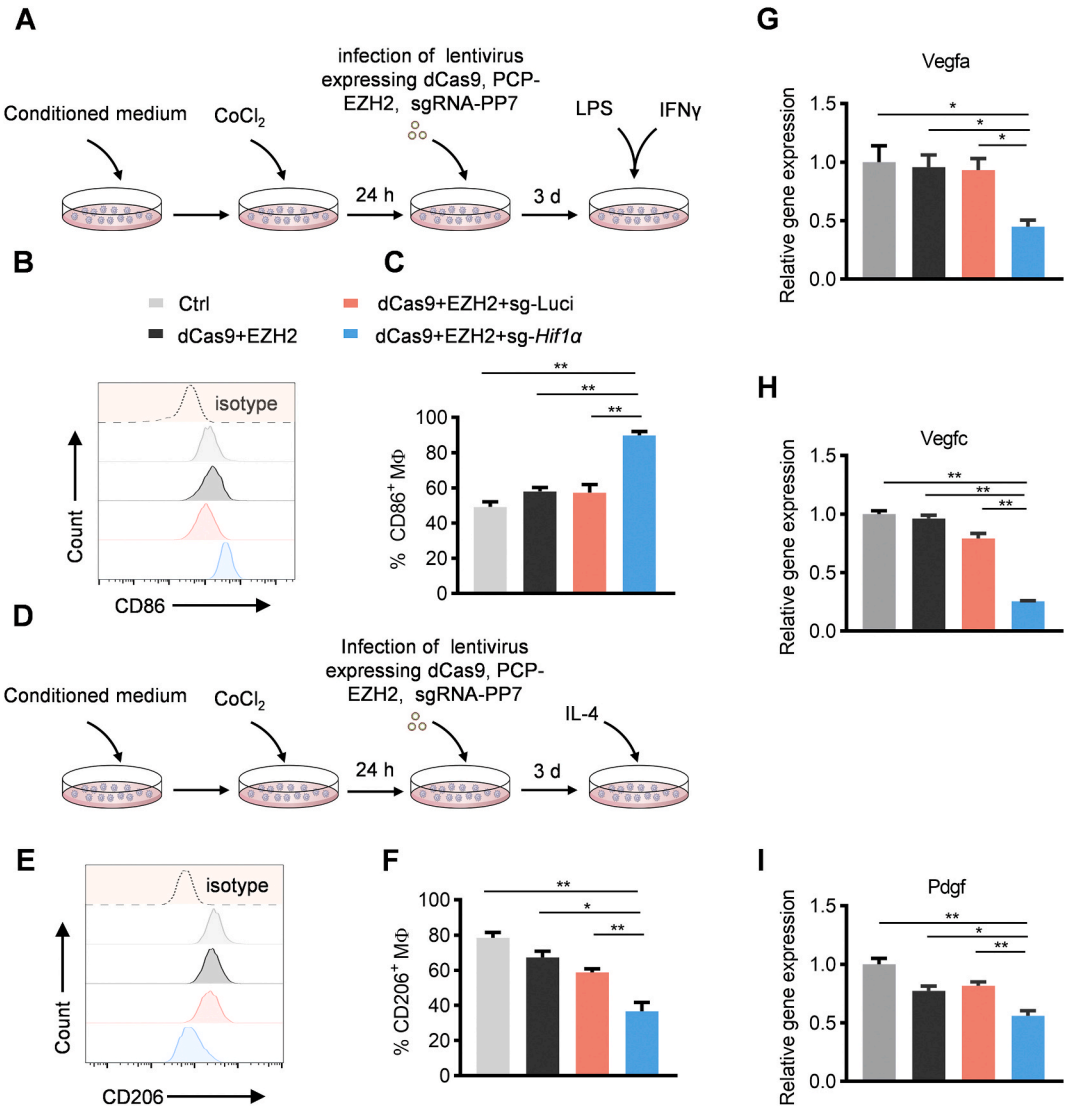

Fig. 4. Phenotype change of HERMs. (A). Schematic of ex vivo effect of CRISPR/dCas9-EZH2 targeting Hif1α system on M1-like polarization. Firstly, $CoCl_2$ was added in BMDMs cultured in conditioned medium for 24 h before lentivirus infection (Ctrl, no sgRNA, sg-Luci or sg- Hif1α). After 3 days, IFN-γ and LPS were added for induction of M1-like polarization. (B). Flow cytometry analysis of $CD86^+$ macrophages in BMDMs treated above. (C). Quantification of $CD86^+$ macrophages in BMDMs treated as above. Data are expressed as mean ± S.E.M. of three different experiments. $^{**}p < 0.01$. (D). Schematic of ex vivo effect of CRISPR/dCas9-EZH2 targeting Hif1α system on M2-like polarization. $CoCl_2$ was added in BMDMs cultured in conditioned medium for 24 h before lentivirus infection (Ctrl, dCas9+EZH2, dCas9+EZH2+sg-Luci, dCas9+EZH2+sg-HIF1α). After 3 days, IL-4 was added for M2-like polarization. (E). Flow cytometry analysis of $CD206^+$ cells among CD11b+ and $F4/80^+$ cells in BMDMs treated above. (F). Quantification of $CD206^+$ cells among $CD11b^+$ and $F4/80^+$ cells in BMDMs treated above. Data are expressed as mean ± S.E.M. of three different experiments. $^{*}p < 0.05$, $^{**}p < 0.01$ by one-way ANOVA. (G–I). Expression level of *Vegfa, Vegfc, Pdgf* in BMDMs treated same as above. Data are expressed as mean ± S.E.M. of three different experiments. $^{*}p < 0.05$, $^{**}p < 0.01$ by one-way ANOVA.

phagocytosis, control or HERMs were labeled with DiI, while the B16-F10 cells were labeled with DiO, followed by incubation with pirarubicin. Then, the DiI-labeled control or HERMs were cocultured with the DiO-labeled B16-F10 cells (Figure S6A). Fluorescent staining revealed more colocalization of HERMs with B16-F10 cells (Figure S6B), suggesting that epigenetically repress *Hif1α* robustly promoted phagocytosis of macrophage. All of these data indicated that HERMs displayed enhanced M1-like polarization and phagocytosis, suggesting a stronger anti-tumoral function of macrophage *in vivo*.

2.4. HERMs suppress tumor progression in vivo

Given the potent ex vivo effect of HERMs, we evaluated the efficacy of intratumor adoptive transfer of HERMs in the B16-F10 mouse melanoma model. To trace the cell distribution after intratumor adoptive macrophage transfer, GFP labeled bone marrow-derived macrophages from C57BL/6-Tg(CAG-EGFP)1Osb/J transgenic mice were used. As expected, GFP-MΦ were found substantially accumulated in the tumor till 12 d after intratumor injection (Figure S7A-C). Furthermore, there were some injected macrophages redistributed to the spleen and liver after intratumoral injection (Figure S8A-B). However, there were no obvious toxicity observed in the organs for all the control and HERMs, as revealed by HE staining (Figure S9).

Since increased *Hif1α* expression occurred at about day 12 while macrophage polarization changed at about day 16 in the syngeneic model (Figure S1), we thus injected the control macrophages and HERMs at day 12 after inoculation (Fig. 5A). At day 32 after tumor implantation, the total amount of macrophages per tumor were generally comparable (Figure S10). However, there were robustly more M1 and less M2 macrophages in HERMs treated group, when compared with that in $M\Phi^{Ctrl}$, $M\Phi^{dCas9+EZH2}$, $M\Phi^{dCas9+EZH2+sg-Luci}$ groups (Fig. 5B–D). Together, these data show that HERMs were inclined to revert the tumor

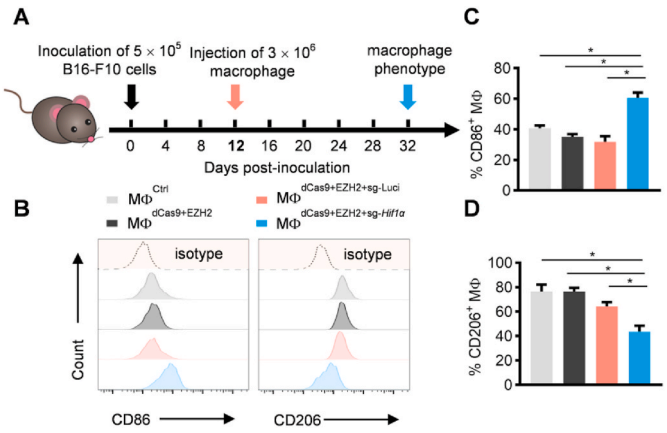

Fig. 5. HERMs treatment remodel the macrophage profile *in vivo*. (A). Schematic of experimental design. Mice were transplanted with 5×10^5 B16-F10 by subcutaneous injection. Macrophages were intratumor injected at 12 days after tumor cell implantation and the phenotype of macrophage was measured at 32 days after implantation. (B). Flow cytometry analysis of $CD86^+$ and $CD206^+$ cells among $CD11b^+$ and $F4/80^+$ cells in tumor tissues injected with Ctrl-MACs, free sgRNA-MACs, sg-Luci-MACs or HERMs. (C and D). Quantification of $CD86^+$ (C) or $CD206^+$ (D) cells among $CD11b^+$ and $F4/80^+$ cells in tumor tissues treated as above (n = 5 mice/group). $^*p < 0.05$.

suppressive microenvironment.

To further analyze the effects of HERMs on tumor progression, luciferase expressing B16-F10 cells were inoculated in C57BL/6J mice (Fig. 6A). Bioluminescence imaging revealed that all mice injected with the HERMs had a visible decrease of tumor size compared to control macrophages (Fig. 6B). Consistently, the tumor mass was much smaller after HERMs treatment (Fig. 6C). Notably, the tumor showed no more growth in mice injected with the HERMs (Fig. 6D). And the mice treated with HERMs had much larger survival rate (Fig. 6E). To study the further immunotherapeutic activity of HERMs, we inoculated B16 melanoma cells bilaterally in syngeneic mice and injected HERMs into the left tumor lesion (Fig. 7A). As expected, injection of HERMs could also initiate anti-tumor immunization and remove remote tumors in the contralateral side (Fig. 7B and C). These data suggest that the HERMs dramatically repress tumor progression.

2.5. Functional mechanisms of HERMs in inhibiting tumor progression

In the following experiments, we asked whether intratumor transfer of the HERMs has positive effects on the immune response to the tumor. To this end, HERMs and control macrophages were injected at 12 days after tumor cell inoculation as mentioned above and the immune response was systemically analyzed at day 32 (Fig. 8A). There were elevated levels of inflammatory cells in tumor injected with the HERMs (Figure S11A-B). Immunofluorescence showed that HERMs treatment significantly enhanced a notable elevation of CD3 positive T cells in tumors (Fig. 8B and C). Similarly, the expression of T cell-related cytokines *Ifn-γ*, *Il-2*, and *Tnfβ* were strikingly increased in the HERMs treatment group (Fig. 8D). Furthermore, flow cytometry results demonstrated that treatment of HERMs led to a significant increase of total T cells, $CD8^+$ T cells (Fig. 8E–I), while the fraction of $CD4^+$ T cells slightly reduced (Fig. 8F, J). Notably, the proliferation marker Ki67 in $CD3^+$ T cells from the tumors was much higher in HERMs group (Fig. 8G, K).

Immune checkpoints and Treg can mediate an immunosuppressive microenvironment and hence significantly limit the efficacy of anti-tumor immune effects [25,26]. We hypothesized that HERMs could unleash the immune suppression by negative regulation of the immune checkpoints and Tregs. Remarkably, treatment of HERMs significantly decreased the expression of PD1 (Fig. 9A, C). Additionally, intratumor adoptive transfer of HERMs decreased the fraction of $FOXP_3^+$ Treg cells (Fig. 9B, D). These data indicated that the HERMs remarkably activate effective T cells and reverse immune suppression via inhibiting immune checkpoint PD-1 and suppressing Tregs. Additionally, treatment of HERMs had significantly reduced blood vessels (Fig. 10A–F). These findings indicate that the HERMs might suppress angiogenesis of melanoma in addition to unleash the tumor immune response.

In this study, we first demonstrated that activated *Hif1α* in TAMs promoted tumor progression by altering the anti-tumoral effect of macrophage. Next, we have engineered macrophages with *Hif1α* silenced via CRISPR/dCas9 mediated EZH2 recruitment on the promoter region. The resultant HERMs significantly repress tumor progression in the following three ways: 1) rescuing the tumoricidal effect of macrophage and promoting phagocytosis of macrophages; 2) activating effective T cells and unleashing immune suppression in the tumor microenvironment; 3) inhibiting tumor angiogenesis (Fig. 10G).

TAMs are the most abundant inflammatory immune cells in the TME, which secret various cytokines, growth factors, chemokines as well as inflammatory mediators. With these factors, TAMs enhance the process

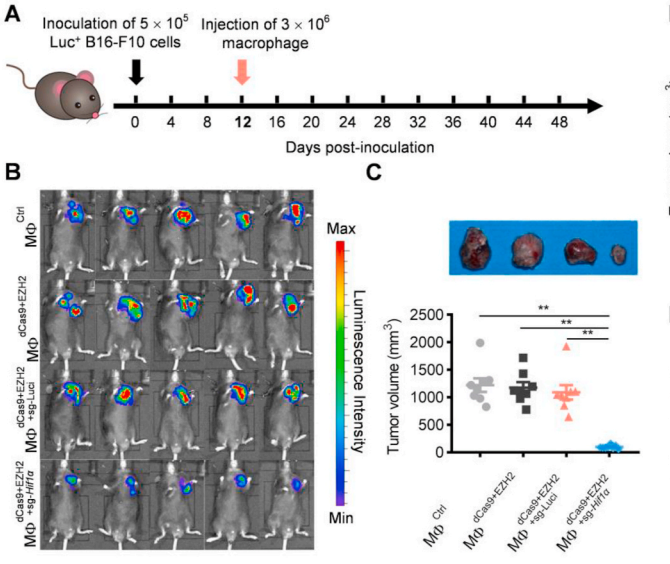

Fig. 6. HERMs inhibit tumor progression in B16-F10 melanoma model. (A). Schematic of experimental design. Mice were transplanted with 5×10^5 B16-F10 transfected with luciferase plasmid by subcutaneous injection. Macrophages were intratumor injected at 12 days after tumor cells implantation and analysis was measured at 48 days after implantation. (B). In vivo fluorescence imaging of C57BL/6 mice injected with B16-F10 cells transfected with luciferase plasmid. Data are expressed as mean ± SEM (n = 5 mice/group). (C). Direct observation of the tumor size treated with $M\Phi^{Ctrl}$, $M\Phi^{dCas9+EZH2}$, $M\Phi^{dCas9+EZH2+sg-Luci}$, the $M\Phi^{dCas9+EZH2+sg-HIF1\alpha}$ (HERM), respectively. Data are expressed as mean ± SEM (n = 8 mice/group). $^{**}p < 0.01$. (D). Tumor growth over time following intratumor injection of $M\Phi^{Ctrl}$, $M\Phi^{dCas9+EZH2}$, $M\Phi^{dCas9+EZH2+sg-Luci}$, the $M\Phi^{dCas9+EZH2+sg-HIF1\alpha}$ (HERM), respectively. (n = 10 mice/group). $^*p < 0.05$, $^{**}p < 0.01$. (E). Mouse survival curve following injection of cells like in (D). (n = 10 mice/group). $^*p < 0.05$.

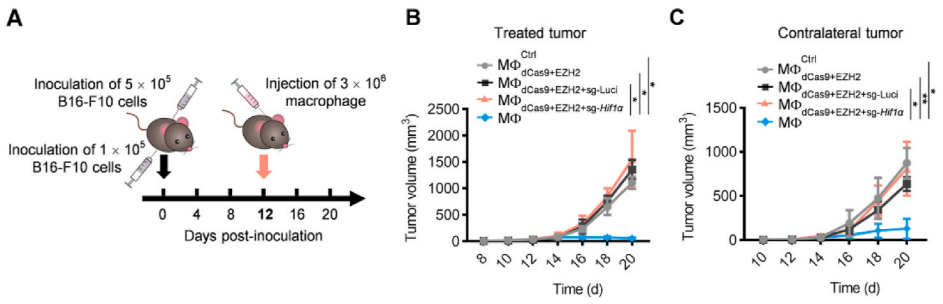

Fig. 7. HERMs inhibit contralateral tumor progression in B16-F10 melanoma model. (A). Schematic of experimental design. Mice were transplanted with B16-F10 cells bilaterally. Macrophages were intratumorally injected into the left tumor at 12 days after tumor cells implantation. (B). Tumor growth in the treatment side over time following intratumoral injection of $M\Phi^{Ctrl}$, $M\Phi^{dCas9+EZH2}$, $M\Phi^{dCas9+EZH2+sg-Luci}$, the $M\Phi^{dCas9+EZH2+sg-HIF1\alpha}$ (HERM), respectively. (n = 5 mice/group). *$p < 0.05$ by two-way ANOVA. (C). Tumor growth in the contralateral side. (n = 5 mice/group). *$p < 0.05$, **$p < 0.01$ by two-way ANOVA.

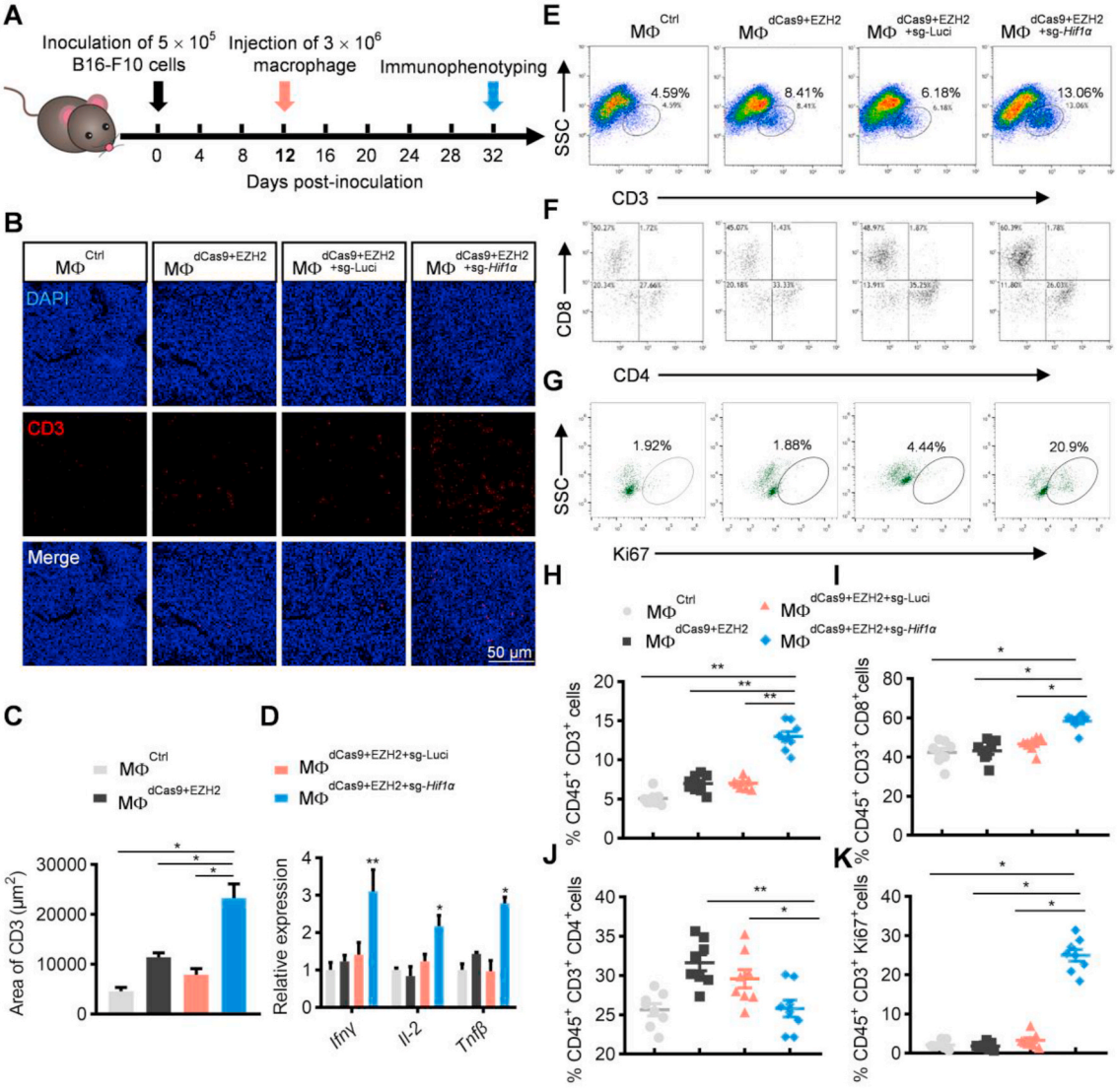

Fig. 8. HERMs activate T cells in the tumor microenvironment. (A). Schematic representation of the experimental design. Mice were transplanted with 5×10^5 B16-F10 by subcutaneous injection. Macrophages were intratumor injected at 12 days after tumor cells implantation and immunophenotype was measured at 32 days after implantation. (B). Immunofluorescence assay of CD3 in tumor tissues treated with $M\Phi^{Ctrl}$, $M\Phi^{dCas9+EZH2}$, $M\Phi^{dCas9+EZH2+sg-Luci}$, the $M\Phi^{dCas9+EZH2+sg-HIF1\alpha}$ (HERM). Images are representative of three independent experiments. Scale bar: 50 μm. (C). Quantification data of B (n = 3 mice/group). *$p < 0.05$ by one-way ANOVA. (D). Expression level of T cell activation cytokines *Ifnγ*, *Il-2*, *Tnfβ* in tumors treated like in B. Data are expressed as mean ± S.E.M. of three different experiments. *$p < 0.05$, **$p < 0.01$ by one-way ANOVA. (E–G). Flow cytometry analysis of CD3 (E), CD4, CD8 (F) and proliferation marker Ki67 (G) in tumor tissues injected with cells like in B. Images are representative of eight independent experiments. (H-K). Quantification data of E-G (n = 8 mice/group). *$p < 0.05$, **$p < 0.01$ by one-way ANOVA.

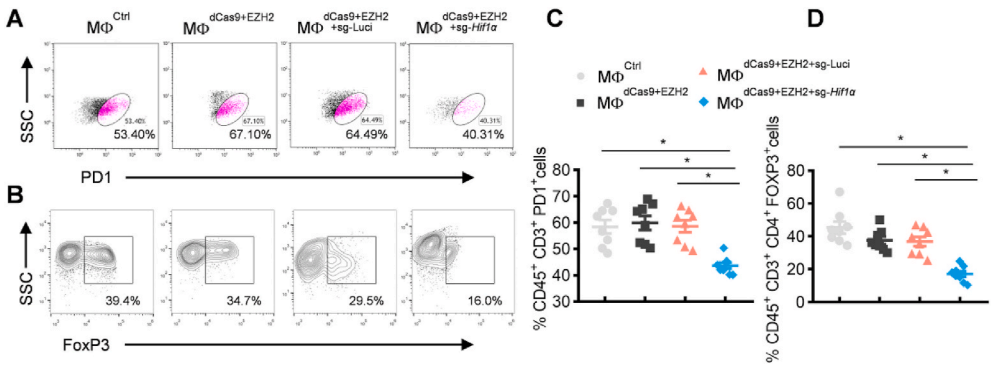

Fig. 9. HERMs unleash immune suppressive microenvironment. (A). Flow cytometry analysis of immune checkpoint PD1 in tumor tissues treated with $M\Phi^{Ctrl}$, $M\Phi^{dCas9+EZH2}$, $M\Phi^{dCas9+EZH2+sg-Luci}$, the $M\Phi^{dCas9+EZH2+sg-HIF1\alpha}$ (HERM). Images are representative of eight independent experiments. (B). Flow cytometry analysis of Treg marker FOXP3 in tumor tissues treated with $M\Phi^{Ctrl}$, $M\Phi^{dCas9+EZH2}$, $M\Phi^{dCas9+EZH2+sg-Luci}$, the $M\Phi^{dCas9+EZH2+sg-HIF1\alpha}$ (HERM). Images are representative of eight independent experiments. (C and D) Quantification data of A and B (n = 8 mice/group). *$p < 0.05$ by one-way ANOVA.

of angiogenesis, invasion, metastasis, and immunosuppression, which allow tumor progression. In situ reprogramming of endogenous TAMs provides an opportunity to rebalance the tumor microenvironment for enhanced cancer immunity. For example, studies have shown that anti-CD47 antibodies [27,28], toll-like receptor agonist [29], anti-CD40 antibodies [30], histone deacetylase inhibitors [31], anti-MARCO antibody therapy [32], PI3Kγ inhibitors [33] and inhibition of related miRNAs [34] are intensively studied strategies for TAMs repolarization [16]. Recently, adoptive macrophage transfer exhibit an effective therapeutic way for liver fibrosis [35], opioid-mediated neuropathic pain [36], multidrug-resistant bacterial sepsis [37], and tuberculosis [38]. What's more, studies demonstrated that injection of ex vivo educated macrophages would hijack existent macrophage recruiting signals and activate immune system to destroy the tumor [39–41]. The macrophage can also be considered as delivery vehicles for loading modified therapeutic micro and nanomaterials for cancer therapy [39,42]. Our study here has further confirmed that adoptive transfer of HERMs into tumor tissues significantly alters TME from immune-suppressive to immune-promoting for enhanced cancer immunotherapy.

Hypoxia is emerging as a hallmark factor of the tumor microenvironment in regulation of glucose metabolism, tumor cell proliferation, differentiation, apoptosis, and angiogenesis [43]. The hypoxia-inducible transcription factors HIF1 and HIF2 are activated under low oxygen tensions associated with tumor progression, metastasis, and therapeutic resistance [44,45]. It has been revealed that HIF1α mediated lactic acid production is able to induce VEGF expression and M2-like polarization in TAMs [46,47]. Beyond hypoxia, some other studies demonstrated that metabolites of tumor microenvironment can stabilize HIF1α, and thus activate M2-polarized macrophages [47,48]. Consistently, we here confirmed that silence of HIF1α could revert the tumor suppressing microenvironment.

It should be noted that a recent excellent study suggested that hypoxia is fine-tune regulator rather than a driving force of TAM subset differentiation in mouse lung carcinoma tumors [49]. In their study, the found that hypoxia is not a major driver of TAM subset differentiation, but rather specifically fine-tunes the phenotype of M2-like MHC-II^{lo} TAM, while the latter is consistent with our study that HERMs enhance the tumor immunity [49]. In another study, hypoxia promoted macrophage polarization towards the M2 phenotype via p38 signaling rather than HIF [50]. The inconsistence might be due to the differences of the tumor type. It is also important to note that hypoxia and glycolysis promotes M1 polarization in sterile inflammation and infection at least via HIF1α [44,51], suggesting the specific role of HIF1α in TAMs. Further clarification of the detailed mechanisms governing the differences would be possibly reveal novel target for macrophage remodeling towards high efficacy and low off-target effects.

In this study, we have revealed that HERMs with HIF1α silenced significantly revert the suppressive immune microenvironment. Beyond skewing the balance between M1 and M2, there should be some other mechanisms for the enhanced cancer immunity. It is widely accepted that TAMs affect immune microenvironment in multiple ways. TAMs-induced immunosuppression is mediated by the expression of inhibitory receptors, including PD-L1, PD-L2 and non-classical major histocompatibility complex (MHC) class I (MHC-I) molecules which inhibit T cells and NK cells functions [26]. TAMs also secrete several cytokines with the function of maintaining a strong immunosuppressive microenvironment by inducing regulatory T (Treg) cell expansion. Furthermore, although antibody-dependent cellular phagocytosis (ADCP) by macrophages functions importantly in the antibody based cancer immunity, ADCP could also induce immunosuppression by inhibiting NK cell-associated antibody-dependent cellular cytotoxicity (ADCC) and T cell-related cytotoxicity, as seen in breast cancers and lymphomas [52]. It is thus interesting to test whether HIF1α interacts with the above molecules or pathways. Notably, HERMs inhibit angiogenesis significantly via VEGF inhibition. It is reasonable to deduce that the remodeled TME might be involved in the role of HERMs reverting the tumor suppressive microenvironment.

As to the engineering strategy, we applied CRISPR/dCas9 based epigenome editing strategy to silence the transcription of HIF1α in macrophages. It is widely accepted that epigenome plays a central role in regulating gene expression associated with numerous disorders including various types of cancers [53]. As more and more epigenetic marks discovered, studies have revealed ubiquitous applicability of epigenetic editing in manipulating gene expression. Engineering of zinc finger proteins (ZFPs) and transcription activator-like effectors (TALEs) are considered as the first gene-editing molecules for site-specific chromatin modifications. However, these protein-DNA interaction-based programmable control requires laborious engineering of different proteins which limits its large-scale applications [54]. Recently developed CRISPR/(d)Cas9 system is becoming the most commonly employed epigenetic editing tool with the advantages of high efficiency, specificity, versatility, and ease of use [55]. In the current study, we silenced HIF1α in macrophages by recruiting H3K27 methyltransferase EZH2 to *Hif1α* promoter with the CRISPR/Cas9 system. Of note, the resultant HERMs are reluctant to hypoxia and the feature could be inheritable to the daughter cells, making the strategy good candidate for adoptive transfer in immunotherapy.

3. Conclusion

In summary, we here identified that HIF1*α* was activated in the tumor associated macrophages and acted as an important factor for the immune suppressive microenvironment. Moreover, we have developed an epigenetically reprogrammed macrophage (HERMs) by targeted silencing *Hif1α* epigenetically in macrophages via CRISPR/dCas9 mediated recruitment of EZH2. Intratumoral injection of the HERMs remarkably restores both the innate and adaptive immune defense, reverts immunosuppression and destroys the tumor. Together, the proposed HERMs set a good example reverting the immune suppressive microenvironment for cancer immunotherapy.

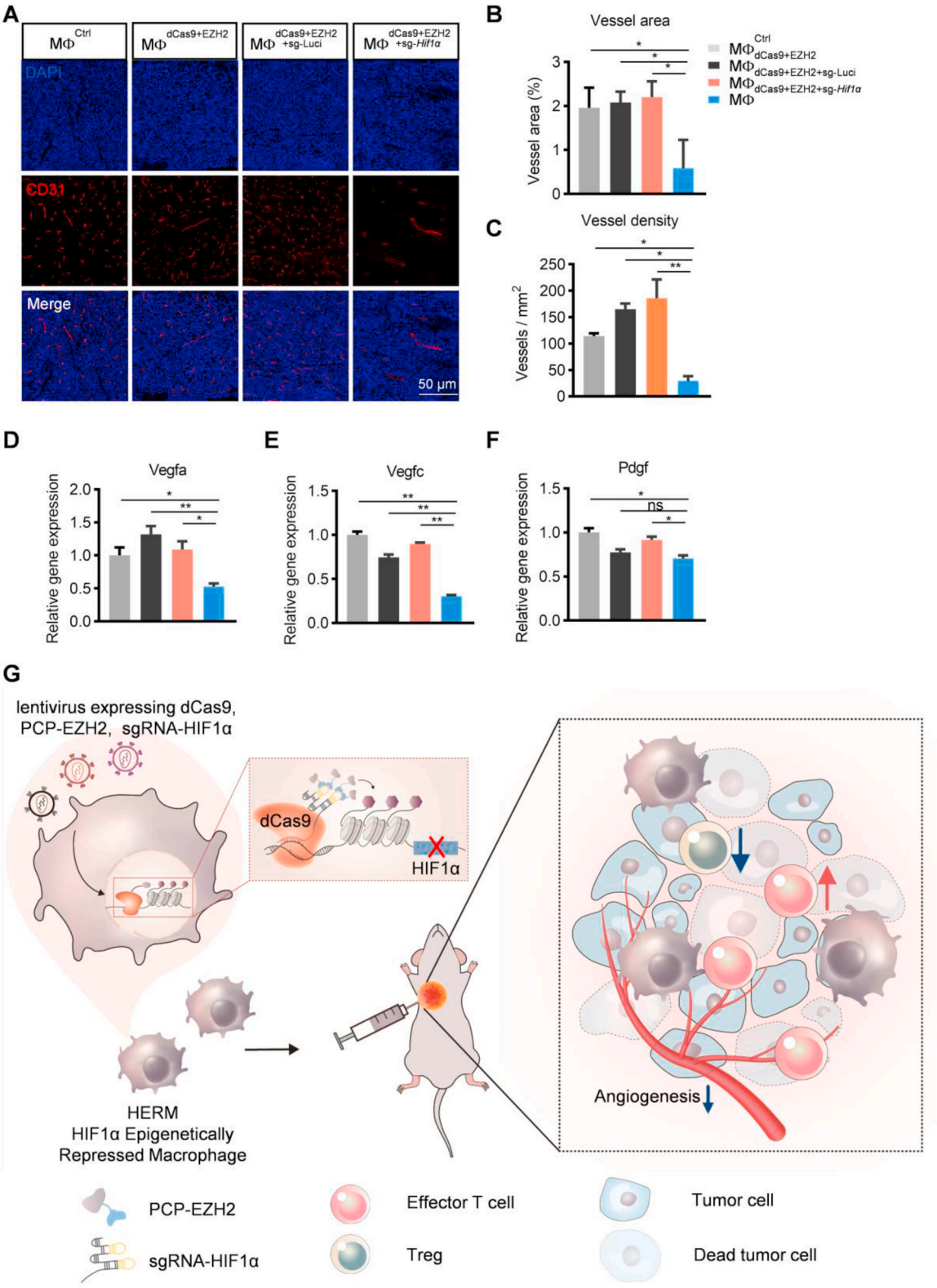

Fig. 10. HERMs inhibit tumor angiogenesis in B16-F10 melanoma model. (A). Representative immunofluorescence images of CD31 expression in tumors injected with $M\Phi^{Ctrl}$, $M\Phi^{dCas9+EZH2}$, $M\Phi^{dCas9+EZH2+sg-Luci}$, $M\Phi^{dCas9+EZH2+sg-HIF1\alpha}$ (HERM). n = 3. Scale bar: 50 μm. (B and C). Quantification data of A (n = 3 mice/group). $^{*}p < 0.05$, $^{**}p < 0.01$ by one-way ANOVA. (D–F). Expression level of *Vegfa, Vegfc, Pdgf* in tumor tissue treated above. Data are expressed as mean ± S.E.M. of three different experiments. $^{*}p < 0.05$, $^{**}p < 0.01$ by *one-way* ANOVA. (G). Graphic illustration of the study. Under hypoxia microenvironment, macrophages are educated to promote cancer progression via inhibiting cancer immunity and enhancing angiogenesis. In contrast, the engineered HERMs (Hif1α Epigenetically Repressed Macrophages) are reluctant to the hypoxic microenvironment and significantly repress tumor progression via unleashing immune suppression and inhibiting tumor angiogenesis.

4. Materials and methods

4.1. Human melanoma samples

Human melanoma samples were obtained from 6 patients with newly diagnosed melanoma. All the patients signed an informed consent form. All specimen acquisition was approved by the Ethics Committee of Fourth Military Medical University.

4.2. Mice

C57BL/6 (8–12 weeks old) male mice were obtained from Fourth Military Medical University. C57BL/6-Tg (CAG-EGFP)1Osb/J mice (stock No: 003291) were purchased from "The Jackson Laboratory". Housing and experimental animal procedures were approved by Animal Experimentation and Ethics Committee of Fourth Military Medical University.

4.3. Bone marrow-derived macrophages (BMDMs) isolation and stimulation

Carbon dioxide was used to euthanize C57/BL6 male mice aged 8–12 weeks. The muscles surrounding the tibia and femur were stripped. The intact tibia and femur were collected in DMEM supplemented with 10% fetal bovine serum and 1% penicillin/streptomycin (Hyclone). Then, the ends of bones were cut and the bone marrow was flushed in a 10 cm plate. The ACK lysis buffer (Sangon Biotech) were added in the plate for 5 min and followed centrifugation of 1000 rpm × 5 min. Next, Bone marrow single cell suspension was plated in a 10 cm plate with bone marrow macrophage generated media (Dulbecco's modified Eagle's medium (DMEM) supplemented with 10% fetal bovine serum, 1% penicillin/streptomycin (Hyclone), and 20 ng/ml M-CSF (Sino Biological Inc. Beijing)). Three days after seeding, an extra 10 mL of fresh media was added and incubated for an additional 3 days. To stimulate BMDMs to M1-or M2-like macrophages, lipopolysaccharide (LPS, 50 ng/ml, Sigma) and IFN-γ (20 ng/ml) or IL-4 (20 ng/ml, PeproTech, Rocky Hill, CT) was added and incubated for 24 h.

4.4. Cell culture

B16-F10 cells, HEK293T cells and RAW 264.7 cells were originally purchased from ATCC. Cell lines were cultured in complete media containing high glucose Dulbecco's modified Eagle medium (DMEM) with 10% fetal bovine serum and 1% penicillin/streptomycin (Hyclone) in a humidified incubator with 5% CO_2 at 37 °C. For hypoxia induction, RAW264.7 or BMDMs were cultured in conditioned DMEM medium containing 150 μM $CoCl_2$ for 24h.

4.5. Plasmid construction

Lentiviral U6-driven sgRNA-PP7 plasmid was generated by replacing sgRNA-MS2 cassette of lenti sgRNA(MS2)_zeo backbone (Addgene #61427) with sgRNA-PP7. The sgRNAs for luciferase gene or *Hif1α* employed in this study were designed according to the SAM protocol (http://sam.genome-engineering.org/protocols/) and can be found in Supplementary Table 1. The nuclease-null dCas9 with point mutations D10A and H840A was amplified from lenti dCAS-VP64_Blast (Addgene #61425) and subcloned into pWPI (Addgene #12254). The plasmid expressing PCP-EZH2 was synthesized in Genscript and subcloned into pWPI plasmid under the EF1α promoter. The sequences and primers used were listed in Supplementary Table 1.

4.6. Lentivirus packaging

HEK293T cells were seeded in 6-well plates and incubated at 60%–80% confluency. Cells were respectively transfected with the target PCP-EZH2, dCas9, sgRNA-luciferase-PP7 and sgRNA-*Hif1α*-PP7 plasmids, and the standard packaging plasmid (psPAX2), envelope plasmid (pMD2.G), and at a 4:3:1 mass ratio by Lipofectamine 2000 (Thermo Fisher) according to the manufacturer's protocol. Cells were then incubated at 37 °C, 5% CO_2 and the lentiviruses in supernatants were collected after 48 h.

4.7. Virus infection and macrophage engineering

RAW 264.7 cells or BMDMs were seeded in 6-well plates and incubated at 37 °C, 5% CO_2 overnight. While approximately 60%–70% were confluent, cells were infected with the lentiviruses expressing PCP-EZH2, dCas9 and sgRNA-PP7 at a 1:1:1 ratio, and medium containing 8 μg/mL polybrene (Sigma, St. Louis, USA). After 24 h infection, cells were replaced with fresh medium.

4.8. Tumor model and intratumor macrophage injection and treatments

C57BL/6 mice were inoculated s. c. with 5×10^5 B16 cells into the right side of the ventral armpit and 1×10^5 B16 cells into the contralateral side The engineered 3×10^6 macrophages were intratumoral injected at the left side 12 days after the construction of the tumor-bearing mouse model. Tumor growth was monitored by measuring tumor length (L) and short (S) with a sliding caliper (tumor size $= L \times S^2 \times 0.5$). At the end of the experiments, the mice were sacrificed, and the tumors were excised for further analysis.

4.9. Western Blotting

Samples were lysed by RIPA buffer with phenylmethylsulfonyl fluoride (PMSF) protease inhibitor (Thermo Fisher). Protein samples were resolved by SDS-PAGE and transferred onto NC membrane. The membrane was first incubated with primary antibodies against HIF1α (1:1000) (Cell Signaling Technology, Danvers, USA), Cas9 (1:1000) (Abcam, Cambridge, UK), PCP (1:1000) (Abcam, Cambridge, UK), or internal control β-actin (Abcam, Cambridge, UK). Then, the membrane was incubated with the secondary antibody (Cell Signaling Technology, Danvers, USA). The bands were visualized by enhanced chemiluminescence assay (ECL, Thermo).

4.10. qRT-PCR assay

Total RNA was isolated from cells of tumor tissues by Tripure Isolation Reagent (Roche, Basel, Switzerland) according to the manufacturer's instructions. Transcriptor Reverse Transcriptase Kit (Roche) was used for total RNA reverse transcription. qRT-PCR was performed using FastStart Essential DNA Green Master Kit (Roche). The sgRNA-luciferase-PP7 and sgRNA-HIF1α-PP7 were measured by qRT-PCR using miRcute miRNA First-Strand cDNA Synthesis Kit and miRcute miRNA SYBR Green qPCR Detection Kit (Tiangen). Data were collected and analyzed using Roche LightCycler 96 qPCR system (Roche). RNA expression was normalized to β-actin or U6 respectively. Relative expression was calculated with the $2^{-\Delta\Delta Ct}$ method. The primers used were listed in Supplementary Table 2.

4.11. Flow cytometry analysis

For flow cytometry, Zombie Violet™ Fixable Viability Kit (BioLegend) or 7AAD Viability Kit (BioLegend) were used as a live/dead marker. The surface stained with the following antibodies obtained from BioLegend: the matching isotype controls, APC/Cyanine7 anti-mouse CD45 Antibody, PE-anti-mouse CD3e, FITC anti-mouse CD4, PE/Cy7 anti-mouse CD8a, Alexa Fluor® 647 anti-mouse CD279 (PD-1), APC-anti-mouse CD11b, FITC-, Percp/Cyanine-anti-mouse-F4/80, PE-anti-mouse CD86, PE-anti-mouse CD206. The intracellular staining cells were firstly permeabilized after surface staining with Intracellular

Staining Perm Wash Buffer (BioLegend) for 20 min according to the manufacturer's instructions and then stained with Alexa Fluor® 647 anti-mouse/human Ki-67, Alexa Fluor® 647 anti-mouse FOXP3.

For flow cytometry of RAW264.7 cells or BMDMs, the CD11b positive and F4/80 positive cells were firstly identified and gated by the expression of CD86 or CD206. Tumor tissues were excised and made into single cell suspensions, the CD45 positive cells were initially identified and gated by the expression of CD4 and CD8, PD1, Ki67, or FOXP3. All samples were performed by the FACS Canto II (BD Biosciences) or CytoFLEX (Beckman Coulter) cytometers. Data were further analyzed by FlowJo V10 software.

4.12. Bioluminescence imaging

The B16-F10 luciferase cell line was generated by stably transfected with luciferase expressing vector pSBbi-pur (Addgene #60523) and pCMV (CAT)T7-SB100 (Addgene #34879) by Lipofectamine 2000 (Thermo Fisher). C57BL/6 (8–12 weeks old) male mice were inoculated with 5×10^5 B16-F10 cells. Twelve days later, mice were injected with engineered macrophages. Four days after macrophage injection, Xeno-Light D-Luciferin Potassium Salt (PerkinElmer) was intra-peritoneally injected at 10 μL/g of body weight for each mouse. Images were detected by an IVIS Lumina II *in vivo* imaging system (PerkinElmer, Thermo Fisher, US) 10–15 min after injection.

4.13. Examination of macrophage phagocytosis

The RAW 264.7 cells were infected with lentivirus expressing PCP-EZH2, dCas9 and sgRNA-PP7 plasmids. Three days later, pretreated RAW264.7 cells were labeled with 5 μM DiI (Life Technologies). Meanwhile, B16-F10 cells were labeled by incubation with 5 μM DiO (Life Technologies). And then, 10 μM pirarubicin (Sigma) was added in B16-F10 cells for 2 days. The DiI-labeled RAW264.7 cells were scraped from the plate, followed by addition into the plate with DiO-labeled B16-F10 cells. After 4 h co-culture, cells were washed and fixed in 4% PFA (Sigma) for 15 min before labeled nuclei by DAPI (Sigma). Samples were observed by a Nikon A1 Spectral Confocal Microscope (Nikon).

4.14. H&E staining and immunofluorescence

Mice were sacrificed and tissues of interest were dissected. Tissues were fixed in 4% PFA (Thermo Fisher), mounted in paraffin blocks, and sliced at 8 μm. The sections of the tissues were stained with H&E. For antibody blockade, the sections were blocked with 5% normal goat serum (Gibco) or CD68 (Abcam), HIF1α (CST) F4/80 (Abcam), CD31 (Abcam), CD3 (Abcam). Images were observed by a Nikon A1 Spectral Confocal Microscope (Nikon).

4.15. Statistics

Results were expressed as mean ± SD or mean ± SEM as indicated and analyzed by student's t-test for two-group comparison or ANOVA for more than three groups. Significance for survival was analyzed by Kaplan-Meier with log-rank analysis. Differences were considered to be significant at $P < 0.05$.

CRediT authorship contribution statement

Yan Dong: conceived the idea, designed the experiments, wrote the original draft, performed the experiments, analyzed the data. **Siyan Zhang:** conceived the idea, designed the experiments, performed the experiments, analyzed the data and commented on the manuscript. **Xiaotong Gao:** designed the experiment, performed the experiments, analyzed the data, discussed the results, reviewed the manuscript. **Dandan Yin:** performed the experiments, discussed the results and commented on the manuscript. **Tingting Wang:** performed the experiments, discussed the results and commented on the manuscript. **Zhelong Li:** gave assistance, discussed the results and commented on the manuscript. **Zhuo Wan:** gave assistance, discussed the results and commented on the manuscript. **Mengying Wei:** gave assistance, discussed the results and commented on the manuscript. **Ying Luo:** designed the experiments, reviewed and edited the manuscript, discussed the results and commented on the manuscript. **Guodong Yang:** conceived the projects, designed the experiments, reviewed and edited the manuscript, discussed the results and commented on the manuscript. **Li Liu:** conceived the projects, designed the experiments, reviewed and edited the manuscript, discussed the results and commented on the manuscript.

Declaration of competing interest

The authors declare that they have no known competing financial interests or personal relationships that could have appeared to influence the work reported in this paper.

Acknowledgements

The authors are grateful to Fan Lu for her assistance with the Nikon microscope system. This work was funded by the National Natural Science Foundation of China (NSFC31573244 to L Liu, NSFC31771507 and NSFC81970737 to G Yang), Key Projects of Shaanxi Province (2018ZDXM-SF-063 to L Liu).

Appendix A. Supplementary data

Supplementary data to this article can be found online at https://doi.org/10.1016/j.bioactmat.2021.02.008.

References

[1] L. Galluzzi, T.A. Chan, G. Kroemer, J.D. Wolchok, A. Lopez-Soto, The hallmarks of successful anticancer immunotherapy, Sci. Transl. Med. 10 (459) (2018).
[2] H. Tang, J. Qiao, Y.X. Fu, Immunotherapy and tumor microenvironment, Canc. Lett. 370 (1) (2016) 85–90.
[3] L. Gu, D.J. Mooney, Biomaterials and emerging anticancer therapeutics: engineering the microenvironment, Nat. Rev. Canc. 16 (1) (2016) 56–66.
[4] P. Gotwals, S. Cameron, D. Cipolletta, V. Cremasco, A. Crystal, B. Hewes, B. Mueller, S. Quaratino, C. Sabatos-Peyton, L. Petruzzelli, J.A. Engelman, G. Dranoff, Prospects for combining targeted and conventional cancer therapy with immunotherapy, Nat. Rev. Canc. 17 (5) (2017) 286–301.
[5] M. De Palma, C.E. Lewis, Cancer: macrophages limit chemotherapy, Nature 472 (7343) (2011) 303–304.
[6] M. Tariq, J. Zhang, G. Liang, L. Ding, Q. He, B. Yang, Macrophage polarization: anti-cancer strategies to target tumor-associated macrophage in breast cancer, J. Cell. Biochem. 118 (9) (2017) 2484–2501.
[7] Y.W. Choo, M. Kang, H.Y. Kim, J. Han, S. Kang, J.R. Lee, G.J. Jeong, S.P. Kwon, S. Y. Song, S. Go, M. Jung, J. Hong, B.S. Kim, M1 macrophage-derived nanovesicles potentiate the anticancer efficacy of immune checkpoint inhibitors, ACS Nano 12 (9) (2018) 8977–8993.
[8] M. De Palma, C.E. Lewis, Macrophage regulation of tumor responses to anticancer therapies, Canc. Cell 23 (3) (2013) 277–286.
[9] C. Murdoch, C.E. Lewis, Macrophage migration and gene expression in response to tumor hypoxia, Int. J. Canc. 117 (5) (2005) 701–708.
[10] H.Z. Imtiyaz, E.P. Williams, M.M. Hickey, S.A. Patel, A.C. Durham, L.-J. Yuan, R. Hammond, P.A. Gimotty, B. Keith, M.C. Simon, Hypoxia-inducible factor 2α regulates macrophage function in mouse models of acute and tumor inflammation, J. Clin. Invest. 120 (8) (2010).
[11] X. Wang, G. Luo, K. Zhang, J. Cao, C. Huang, T. Jiang, B. Liu, L. Su, Z. Qiu, Hypoxic tumor-derived exosomal miR-301a mediates M2 macrophage polarization via PTEN/PI3Kγ to promote pancreatic cancer metastasis, Canc. Res. 78 (16) (2018) 4586–4598.
[12] E.N. Arwert, A.S. Harney, D. Entenberg, Y. Wang, E. Sahai, J.W. Pollard, J. S. Condeelis, A unidirectional transition from migratory to perivascular macrophage is required for tumor cell intravasation, Cell Rep. 23 (5) (2018) 1239–1248.
[13] M. Marra, G. Salzano, C. Leonetti, P. Tassone, M. Scarsella, S. Zappavigna, T. Calimeri, R. Franco, G. Liguori, G. Cigliana, R. Ascani, M.I. La Rotonda, A. Abbruzzese, P. Tagliaferri, M. Caraglia, G. De Rosa, Nanotechnologies to use bisphosphonates as potent anticancer agents: the effects of zoledronic acid encapsulated into liposomes, Nanomed. Nanotechnol. Biol. Med. 7 (6) (2011) 955–964.

[14] P.A. Cassier, A. Italiano, C.A. Gomez-Roca, C. Le Tourneau, M. Toulmonde, M. A. Cannarile, C. Ries, A. Brillouet, C. Muller, A.M. Jegg, A.M. Broske, M. Dembowski, K. Bray-French, C. Freilinger, G. Meneses-Lorente, M. Baehner, R. Harding, J. Ratnayake, K. Abiraj, N. Gass, K. Noh, R.D. Christen, L. Ukarma, E. Bompas, J.P. Delord, J.Y. Blay, D. Ruttinger, CSF1R inhibition with emactuzumab in locally advanced diffuse-type tenosynovial giant cell tumours of the soft tissue: a dose-escalation and dose-expansion phase 1 study, the Lancet, Oncology 16 (8) (2015) 949–956.
[15] K. Weiskopf, A.M. Ring, C.C. Ho, J.P. Volkmer, A.M. Levin, A.K. Volkmer, E. Ozkan, N.B. Fernhoff, M. van de Rijn, I.L. Weissman, K.C. Garcia, Engineered SIRPalpha variants as immunotherapeutic adjuvants to anticancer antibodies, Science (New York, N.Y.) 341 (6141) (2013) 88–91.
[16] L. Cassetta, J.W. Pollard, Targeting Macrophages: Therapeutic Approaches in Cancer, Nature Reviews. Drug Discovery, 2018.
[17] I. Vitale, G. Manic, L.M. Coussens, G. Kroemer, L. Galluzzi, Macrophages and metabolism in the tumor microenvironment, Cell Metabol. 30 (1) (2019) 36–50.
[18] J. Hu, Y. Lei, W.K. Wong, S. Liu, K.C. Lee, X. He, W. You, R. Zhou, J.T. Guo, X. Chen, X. Peng, H. Sun, H. Huang, H. Zhao, B. Feng, Direct activation of human and mouse Oct4 genes using engineered TALE and Cas9 transcription factors, Nucleic Acids Res. 42 (7) (2014) 4375–4390.
[19] A. Mahas, C. Neal Stewart Jr., M.M. Mahfouz, Harnessing CRISPR/Cas systems for programmable transcriptional and post-transcriptional regulation, Biotechnol. Adv. 36 (1) (2018) 295–310.
[20] S.H. Stricker, A. Koferle, S. Beck, From profiles to function in epigenomics, Nat. Rev. Genet. 18 (1) (2017) 51–66.
[21] M. Elsner, Epigenome editing to the rescue, Nat. Biotechnol. 36 (4) (2018) 315.
[22] C.A. Corzo, T. Condamine, L. Lu, M.J. Cotter, J.I. Youn, P. Cheng, H.I. Cho, E. Celis, D.G. Quiceno, T. Padhya, T.V. McCaffrey, J.C. McCaffrey, D.I. Gabrilovich, HIF-1α regulates function and differentiation of myeloid-derived suppressor cells in the tumor microenvironment, J. Exp. Med. 207 (11) (2010) 2439–2453.
[23] D. Wang, J. Quiros, K. Mahuron, C.C. Pai, V. Ranzani, A. Young, S. Silveria, T. Harwin, A. Abnousian, M. Pagani, M.D. Rosenblum, F. Van Gool, L. Fong, J. A. Bluestone, M. DuPage, Targeting EZH2 reprograms intratumoral regulatory T cells to enhance cancer immunity, Cell Rep. 23 (11) (2018) 3262–3274.
[24] S. Konermann, M.D. Brigham, A.E. Trevino, J. Joung, O.O. Abudayyeh, C. Barcena, P.D. Hsu, N. Habib, J.S. Gootenberg, H. Nishimasu, O. Nureki, F. Zhang, Genome-scale transcriptional activation by an engineered CRISPR-Cas9 complex, Nature 517 (7536) (2015) 583–588.
[25] M. Di Pilato, E.Y. Kim, B.L. Cadilha, J.N. Prussmann, M.N. Nasrallah, D. Seruggia, S.M. Usmani, S. Misale, V. Zappulli, E. Carrizosa, V. Mani, M. Ligorio, R.D. Warner, B.D. Medoff, F. Marangoni, A.C. Villani, T.R. Mempel, Targeting the CBM complex causes Treg cells to prime tumours for immune checkpoint therapy, Nature 570 (7759) (2019) 112–116.
[26] S.R. Gordon, R.L. Maute, B.W. Dulken, G. Hutter, B.M. George, M.N. McCracken, R. Gupta, J.M. Tsai, R. Sinha, D. Corey, A.M. Ring, A.J. Connolly, I.L. Weissman, PD-1 expression by tumour-associated macrophages inhibits phagocytosis and tumour immunity, Nature 545 (7655) (2017) 495–499.
[27] M.P. Chao, A.A. Alizadeh, C. Tang, J.H. Myklebust, B. Varghese, S. Gill, M. Jan, A. C. Cha, C.K. Chan, B.T. Tan, C.Y. Park, F. Zhao, H.E. Kohrt, R. Malumbres, J. Briones, R.D. Gascoyne, I.S. Lossos, R. Levy, I.L. Weissman, R. Majeti, Anti-CD47 antibody synergizes with rituximab to promote phagocytosis and eradicate non-Hodgkin lymphoma, Cell 142 (5) (2010) 699–713.
[28] S.B. Willingham, J.P. Volkmer, A.J. Gentles, D. Sahoo, P. Dalerba, S.S. Mitra, J. Wang, H. Contreras-Trujillo, R. Martin, J.D. Cohen, P. Lovelace, F.A. Scheeren, M.P. Chao, K. Weiskopf, C. Tang, A.K. Volkmer, T.J. Naik, T.A. Storm, A.R. Mosley, B. Edris, S.M. Schmid, C.K. Sun, M.S. Chua, O. Murillo, P. Rajendran, A.C. Cha, R. K. Chin, D. Kim, M. Adorno, T. Raveh, D. Tseng, S. Jaiswal, P. Enger, G. K. Steinberg, G. Li, S.K. So, R. Majeti, G.R. Harsh, M. van de Rijn, N.N. Teng, J. B. Sunwoo, A.A. Alizadeh, M.F. Clarke, I.L. Weissman, The CD47-signal regulatory protein alpha (SIRPa) interaction is a therapeutic target for human solid tumors, Proc. Natl. Acad. Sci. U. S. A 109 (17) (2012) 6662–6667.
[29] S. Adams, L. Kozhaya, F. Martiniuk, T.C. Meng, L. Chiriboga, L. Liebes, T. Hochman, N. Shuman, D. Axelrod, J. Speyer, Y. Novik, A. Tiersten, J. D. Goldberg, S.C. Formenti, N. Bhardwaj, D. Unutmaz, S. Demaria, Topical TLR7 agonist imiquimod can induce immune-mediated rejection of skin metastases in patients with breast cancer, Clin. Canc. Res. 18 (24) (2012) 6748–6757, an official journal of the American Association for Cancer Research.
[30] S. Hoves, C.H. Ooi, C. Wolter, H. Sade, S. Bissinger, M. Schmittnaegel, O. Ast, A. M. Giusti, K. Wartha, V. Runza, W. Xu, Y. Kienast, M.A. Cannarile, H. Levitsky, S. Romagnoli, M. De Palma, D. Rüttinger, C.H. Ries, Rapid activation of tumor-associated macrophages boosts preexisting tumor immunity, J. Exp. Med. 215 (3) (2018) 859–876.
[31] J.L. Guerriero, A. Sotayo, H.E. Ponichtera, J.A. Castrillon, A.L. Pourzia, S. Schad, S. F. Johnson, R.D. Carrasco, S. Lazo, R.T. Bronson, S.P. Davis, M. Lobera, M. A. Nolan, A. Letai, Class IIa HDAC inhibition reduces breast tumours and metastases through anti-tumour macrophages, Nature 543 (7645) (2017) 428–432.
[32] F. Li, J.V. Ravetch, Inhibitory Fcγ receptor engagement drives adjuvant and anti-tumor activities of agonistic CD40 antibodies, Science (New York, N.Y.) 333 (6045) (2011) 1030–1034.
[33] M.M. Kaneda, K.S. Messer, N. Ralainirina, H. Li, C.J. Leem, S. Gorjestani, G. Woo, A.V. Nguyen, C.C. Figueiredo, P. Foubert, M.C. Schmid, M. Pink, D.G. Winkler, M. Rausch, V.J. Palombella, J. Kutok, K. McGovern, K.A. Frazer, X. Wu, M. Karin, R. Sasik, E.E. Cohen, J.A. Varner, PI3Kγ is a molecular switch that controls immune suppression, Nature 539 (7629) (2016) 437–442.
[34] C. Baer, M.L. Squadrito, D. Laoui, D. Thompson, S.K. Hansen, A. Kiialainen, S. Hoves, C.H. Ries, C.H. Ooi, M. De Palma, Suppression of microRNA activity amplifies IFN-γ-induced macrophage activation and promotes anti-tumour immunity, Nat. Cell Biol. 18 (7) (2016) 790–802.
[35] P.F. Ma, C.C. Gao, J. Yi, J.L. Zhao, S.Q. Liang, Y. Zhao, Y.C. Ye, J. Bai, Q.J. Zheng, K.F. Dou, H. Han, H.Y. Qin, Cytotherapy with M1-polarized macrophages ameliorates liver fibrosis by modulating immune microenvironment in mice, J. Hepatol. 67 (4) (2017) 770–779.
[36] M. Pannell, D. Labuz, M. Celik, J. Keye, A. Batra, B. Siegmund, H. Machelska, Adoptive transfer of M2 macrophages reduces neuropathic pain via opioid peptides, J. Neuroinflammation 13 (1) (2016) 262.
[37] X. Hou, X. Zhang, W. Zhao, C. Zeng, B. Deng, D.W. McComb, S. Du, C. Zhang, W. Li, Y. Dong, Vitamin lipid nanoparticles enable adoptive macrophage transfer for the treatment of multidrug-resistant bacterial sepsis, Nat. Nnanotechnol. 15 (1) (2020) 41–46.
[38] E. Kaufmann, J. Sanz, J.L. Dunn, N. Khan, L.E. Mendonça, A. Pacis, F. Tzelepis, E. Pernet, A. Dumaine, J.C. Grenier, F. Mailhot-Léonard, E. Ahmed, J. Belle, R. Besla, B. Mazer, I.L. King, A. Nijnik, C.S. Robbins, L.B. Barreiro, M. Divangahi, BCG educates hematopoietic stem cells to generate protective innate immunity against tuberculosis, Cell 172 (1–2) (2018) 176–190, e19.
[39] S. Lee, S. Kivimäe, A. Dolor, F.C. Szoka, Macrophage-based cell therapies: the long and winding road, J. Contr. Release 240 (2016) 527–540, official journal of the Controlled Release Society.
[40] R. Andreesen, C. Scheibenbogen, W. Brugger, S. Krause, H.G. Meerpohl, H.G. Leser, H. Engler, G.W. Lohr, Adoptive transfer of tumor cytotoxic macrophages generated in vitro from circulating blood monocytes: a new approach to cancer immunotherapy, Canc. Res. 50 (23) (1990) 7450–7456.
[41] R. Andreesen, B. Hennemann, S.W. Krause, Adoptive immunotherapy of cancer using monocyte-derived macrophages: rationale, current status, and perspectives, J. Leukoc. Biol. 64 (4) (1998) 419–426.
[42] E.C. Wayne, C. Long, M.J. Haney, E.V. Batrakova, T.M. Leisner, L.V. Parise, A. V. Kabanov, Targeted delivery of siRNA lipoplexes to cancer cells using macrophage transient horizontal gene transfer, Adv. Sci. (Weinheim, Baden-Wurttemberg, Germany) 6 (21) (2019) 1900582.
[43] A.T. Henze, M. Mazzone, The impact of hypoxia on tumor-associated macrophages, J. Clin. Invest. 126 (10) (2016) 3672–3679.
[44] N. Takeda, E.L. O'Dea, A. Doedens, J.W. Kim, A. Weidemann, C. Stockmann, M. Asagiri, M.C. Simon, A. Hoffmann, R.S. Johnson, Differential activation and antagonistic function of HIF-{alpha} isoforms in macrophages are essential for NO homeostasis, Genes Dev. 24 (5) (2010) 491–501.
[45] E.B. Rankin, A.J. Giaccia, Hypoxic control of metastasis, Science (New York, N.Y.) 352 (6282) (2016) 175–180.
[46] O.R. Colegio, N.Q. Chu, A.L. Szabo, T. Chu, A.M. Rhebergen, V. Jairam, N. Cyrus, C.E. Brokowski, S.C. Eisenbarth, G.M. Phillips, G.W. Cline, A.J. Phillips, R. Medzhitov, Functional polarization of tumour-associated macrophages by tumour-derived lactic acid, Nature 513 (7519) (2014) 559–563.
[47] K. Mehla, P.K. Singh, Metabolic regulation of macrophage polarization in cancer, Trends Canc. 5 (12) (2019) 822–834.
[48] P.S. Liu, H. Wang, X. Li, T. Chao, T. Teav, S. Christen, G. Di Conza, W.C. Cheng, C. H. Chou, M. Vavakova, C. Muret, K. Debackere, M. Mazzone, H.D. Huang, S. M. Fendt, J. Ivanisevic, P.C. Ho, α-ketoglutarate orchestrates macrophage activation through metabolic and epigenetic reprogramming, Nat. Immunol. 18 (9) (2017) 985–994.
[49] D. Laoui, E. Van Overmeire, G. Di Conza, C. Aldeni, J. Keirsse, Y. Morias, K. Movahedi, I. Houbracken, E. Schouppe, Y. Elkrim, O. Karroum, B. Jordan, P. Carmeliet, C. Gysemans, P. De Baetselier, M. Mazzone, J.A. Van Ginderachter, Tumor hypoxia does not drive differentiation of tumor-associated macrophages but rather fine-tunes the M2-like macrophage population, Canc. Res. 74 (1) (2014) 24–30.
[50] X. Ke, C. Chen, Y. Song, Q. Cai, J. Li, Y. Tang, X. Han, W. Qu, A. Chen, H. Wang, G. Xu, D. Liu, Hypoxia modifies the polarization of macrophages and their inflammatory microenvironment, and inhibits malignant behavior in cancer cells, Oncol. Lett. 18 (6) (2019) 5871–5878.
[51] A. Egners, M. Erdem, T. Cramer, The response of macrophages and neutrophils to hypoxia in the context of cancer and other inflammatory diseases, Mediat. Inflamm. 2016 (2016) 2053646.
[52] S. Su, J. Zhao, Y. Xing, X. Zhang, J. Liu, Q. Ouyang, J. Chen, F. Su, Q. Liu, E. Song, Immune checkpoint inhibition overcomes ADCP-induced immunosuppression by macrophages, Cell 175 (2) (2018) 442–457, e23.
[53] L. Holtzman, C.A. Gersbach, Editing the epigenome: reshaping the genomic landscape, Annu. Rev. Genom. Hum. Genet. 19 (2018) 43–71.
[54] P.I. Thakore, J.B. Black, I.B. Hilton, C.A. Gersbach, Editing the epigenome: technologies for programmable transcription and epigenetic modulation, Nat. Methods 13 (2) (2016) 127–137.
[55] J. Pulecio, N. Verma, E. Mejía-Ramírez, D. Huangfu, A. Raya, CRISPR/Cas9-Based engineering of the epigenome, Cell Stem Cell 21 (4) (2017) 431–447.